Heavy-residue isoscaling as a probe of the symmetry energy of hot fragments

G. A. Souliotis, D. V. Shetty, A. Keksis, E. Bell, M. Jandel, M. Veselsky,* and S. J. Yennello
Cyclotron Institute, Texas A&M University, College Station, TX 77843
(Dated: May 10, 2018)

The isoscaling properties of isotopically resolved projectile residues from peripheral collisions of ^{86}Kr (25 MeV/nucleon), ^{64}Ni (25 MeV/nucleon) and ^{136}Xe (20 MeV/nucleon) beams on various target pairs are employed to probe the symmetry energy coefficient of the nuclear binding energy. The present study focuses on heavy projectile fragments produced in peripheral and semiperipheral collisions near the onset of multifragment emission (E^*/A = 2–3 MeV). For these fragments, the measured average velocities are used to extract excitation energies. The excitation energies, in turn, are used to estimate the temperatures of the fragmenting quasiprojectiles in the framework the Fermi gas model. The isoscaling analysis of the fragment yields provided the isoscaling parameters α which, in combination with temperatures and isospin asymmetries provided the symmetry energy coefficient of the nuclear binding energy of the hot fragmenting quasiprojectiles. The extracted values of the symmetry energy coefficient at this excitation energy range (2–3 MeV/nucleon) are lower than the typical liquid-drop model value $\sim$ 25 MeV corresponding to ground-state nuclei and show a monotonic decrease with increasing excitation energy. This result is of importance in the formation of hot nuclei in heavy-ion reactions and in hot stellar environments such as supernova.

PACS numbers: 25.70.Mn,25.70.Lm,25.70.Pq

I. INTRODUCTION

The study of the nuclear symmetry energy is currently a topic of intense theoretical and experimental work. It is well established that the symmetry energy plays a central role in a variety of astrophysical phenomena including the structure and evolution of neutron stars and the dynamics of supernova explosions [1, 2, 3, 4, 5, 6, 7, 8]. In addition, the symmetry energy determines the nuclear structure of neutron-rich or neutron deficient rare isotopes [9, 10, 11, 12].

The symmetry energy at normal nuclear density has been obtained from a number of many-body approaches [13, 14, 15, 16, 17] and from nuclear mass systematics [18, 19, 20, 21]. However, its values at densities below or above the normal nuclear density are not adequately constrained [22, 23, 24]. Indeed, the experimental determination of the symmetry energy and its density dependence is a challenging scientific endeavor. Information on the symmetry energy can be gleaned from the determination of the neutron skins of neutron-rich nuclei [9], from elastic scattering on neutron-rich nuclei [25] and from heavy-ion collisions. For the latter, a great deal of effort is currently devoted in order to identify observables sensitive to the nuclear symmetry energy and its density dependence (see, e.g., [24, 26, 27, 28, 29]).

One important observable in heavy ion collisions is the fragment isotopic composition investigated with the recently developed isoscaling approach [30]. The isoscaling approach attempts to isolate the effects of the nuclear symmetry energy in the fragment yields, thus allowing a direct study of the role of this term of the nuclear binding energy in the formation of hot fragments. Isoscaling refers to a general exponential relation between the yields of a given fragment from two reactions that differ only in their isospin asymmetry (N/Z) [30, 31, 32]. In particular, if two reactions, 1 and 2, lead to primary fragments having approximately the same temperature but different isospin asymmetry, the ratio R_{21}(N,Z) of the yields of a given fragment (N,Z) from these primary fragments exhibits an exponential dependence on the neutron number N and the atomic number Z of the form:

$$R_{21}(N,Z) = C\exp(\alpha N + \beta Z) \quad (1)$$

where α and β are the scaling parameters and C is a normalization constant. This scaling behavior has been observed in a very broad range of reactions including evaporation [30, 32], fission [33, 34], deep-inelastic reactions [30, 35, 36] and multifragmentation [30, 32, 37, 38, 39, 40, 41]. In the initial studies of isoscaling, it was shown that the isoscaling parameters are almost unaffected by the sequential decay of the primary fragments, due to possibly similar de-excitation paths of the two primary fragments, thus they could provide information on the early stage of fragment formation. In particular, within the statistical framework, the isoscaling parameter α is linearly related to the symmetry energy coefficient of the fragment binding energy [28, 30, 32, 42]. This relation provides the key connection of the measured isoscaling parameter with the symmetry energy coefficient.

In the present work, the isoscaling properties of isotopically resolved projectile residues from peripheral collisions of ^{86}Kr (25 MeV/nucleon), ^{64}Ni (25 MeV/nucleon) and ^{136}Xe (20 MeV/nucleon) beams on a variety of target pairs are employed to probe the symmetry energy coefficient of the nuclear binding energy. The collection and complete characterization of the residues in terms

*Institute of Physics of the Slovak Academy of Sciences, Bratislava, Slovakia.

of their atomic number Z, mass number A and velocity has been performed with the use of two magnetic separators: the MARS recoil separator and the Superconducting Solenoid Line at Texas A&M University. In this work, apart from isotopically resolved yields, the velocities of the fragments are obtained with high resolution and are used to provide information on the excitation energy (and temperature) of the primary fragments. The isoscaling parameters α along with temperatures and isospin asymmetries yielded the values of the nuclear symmetry energy in the excitation energy range 2–3 MeV/nucleon. The paper is organized as follows. In Section II, a brief description of the experimental devices, the measurements and the data analysis is given. In Section III, the isotopic scaling of the fragment yields and the velocity distributions are presented. In Section IV, the systematics of the isoscaling parameter α with respect to isospin asymmetry is presented and used to get the symmetry energy. Finally, conclusions from the present study are summarized in Section V.

II. EXPERIMENTAL METHODS AND DATA ANALYSIS

The present studies were performed at the Cyclotron Institute of Texas A&M University using two different devices: the MARS recoil separator and the Superconducting Solenoid Line. Below we give a concise description of the measurements with each of these devices.

A. Measurements with the MARS recoil separator

The reactions of ^{86}Kr with ^{64,58}Ni and ^{124,112}Sn were studied with the MARS recoil separator. The general isoscaling analysis of these data has been reported recently [35]. Nevertheless, for a complete presentation of the heavy-residue isoscaling approach to probe the symmetry energy, we briefly summarize the method below. A 25 MeV/nucleon ^{86}Kr beam from the K500 superconducting cyclotron, with a current of $\sim$1 pnA, interacted with isotopically enriched targets of ^{64}Ni, ^{58}Ni and ^{124}Sn, ^{112}Sn. The reaction products entered the MARS spectrometer [43] having an angular acceptance of 9 msr and momentum acceptance of 4%. The primary beam struck the target at 4.0^o relative to the optical axis of the spectrometer. Fragments were accepted in the polar angular range 2.7^o–5.4^o. This angular range lies inside the grazing angle θ_{gr}=6.5^o of the Kr+Sn reactions and mostly outside the grazing angle θ_{gr}=3.5^o of the Kr+Ni reactions at 25 MeV/nucleon [44]. (The spectrometer angle setting was chosen to optimize the production of very neutron-rich fragments from the Kr+Sn systems whose detailed study has been reported in [45].) An Al stripper foil (1 mg/cm^2) was used to reset to equilibrium the ionic charge states of the projectile fragments. MARS optics [43] provides one intermediate dispersive image and one (final) achromatic image (focal plane). At the focal plane, the fragments were collected in a 5×5 cm two-element (ΔE, E) Si detector telescope. Time of flight was measured between two PPACs (Parallel Plate Avalanche Counters) positioned at the dispersive image and at the focal plane, respectively, and separated by a distance of 13.2 m. The PPAC at the dispersive image was also X–Y position sensitive and used to record the position of the fragments. The horizontal position, along with NMR measurements of the field of the MARS first dipole, provided the magnetic rigidity, $B\rho$, of the particles.

The determination of the atomic number Z was based on the energy loss of the particles in the ΔE detector and their velocity. The ionic charge q of the particles entering MARS was obtained from the total energy E$_{tot}$=ΔE + E, the velocity and the magnetic rigidity. The measurements of Z and q had resolutions of 0.5 and 0.4 units (FWHM), respectively. Since the ionic charge is an integer, we assigned integer values of q for each event by putting windows (Δq = 0.4) on each peak of the q spectrum. Using the magnetic rigidity and velocity measurement, the mass-to-charge A/q ratio of each ion was obtained with a resolution of 0.3%. Combining the q determination with the A/q measurement, the mass A was obtained as: $A = q_{int} \times A/q$ (q$_{int}$ is the integer ionic charge) with a resolution (FWHM) of 0.6 A units. Combination and normalization of the data at the various magnetic rigidity settings of the spectrometer (in the range 1.3–2.0 T m), summation over all ionic charge states and, finally, normalization for beam current and target thickness, provided fragment yield distributions with respect to Z, A and velocity. Further details of the analysis procedure can be found in [46, 47]. The yield distributions, summed over velocities, were used to obtain the fragment yield ratios $R_{21}(N,Z) = Y_2(N,Z)/Y_1(N,Z)$ employed in the present isoscaling studies.

B. Measurements with the Superconducting Solenoid Line

The heavy-residue work with the Superconducting Solenoid Line shares many similarities with the previously described work with MARS and it is described below. The complete (two-stage) Superconducting Solenoid Line (Fig. 1) consists of the 7-Tesla superconducting solenoid ("BigSol") of the University of Michigan (first stage) [48, 49] and a large-bore quadrupole triplet (second stage). The whole separator line is also referred to as the "BigSol" line. Details of the development of the line and plans/progress towards producing rare isotopes in deep-inelastic collisions are provided in [47, 50].

In the present isoscaling studies with BigSol, first, the reactions of a ^{64}Ni (25 MeV/nucleon) beam with targets of ^{64,58}Ni, ^{124,112}Sn and ^{208}Pb, ^{232}Th were studied. Second, the reactions of a ^{136}Xe (20 MeV/nucleon) beam with targets of ^{64,58}Ni, ^{124,112}Sn and ^{197}Au, ^{232}Th were

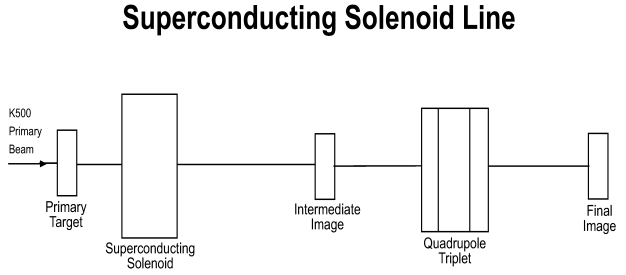

FIG. 1: Schematic diagram of the Superconducting Solenoid Line (BigSol) used in the present heavy residue isoscaling studies (see text)

measured. The typical beam current was ∼1 pnA. The primary beam, after hitting the target, was collected on an on-axis blocker located ∼30 cm after the target. The beam blocker along with a circular aperture at this location defined the angular acceptance of the line to be 1.5^o–3.0^o. The fragments then passed through a stripper foil, traversed the solenoid and were focused at the intermediate image (Fig. 1). At this location, a magnetic rigidity (or momentum-over-charge p/q) acceptance of ∼4% was defined with another circular aperture. Subsequently, the fragments were transported through a 7.5 meter line and focused with the aid of the quadrupole triplet at the end of the line (final image). Time-of-flight was provided between two X-Y position sensitive PPACs, one at the intermediate image and the other at the final image. A silicon detector array similar to the one used in the MARS measurements provided ΔE, E information, which, combined with time-of-flight (with resolution ∼0.5%) provided Z and A determination (with resolutions of 0.5 and 0.6 units, respectively, for Ni-like fragments).

It should be noted that, in contrast to the MARS measurements, here the mass determination was based solely on total energy and time-of-flight. The reason is that BigSol does not provide high-resolution p/q dispersion. The Solenoid Line is not a magnetic spectrometer in the classical sense [51]. Its elements are only focusing elements. There is radial p/q dispersion at the intermediate image due to the solenoid (and, of course, at the final image, due to the quadrupole triplet) as a consequence of the variation of the location of the focus with p/q. This dispersion is also a function of the initial angle [48]. The measurement of the radial distance of the fragments at the intermediate image (emerging, as stated previously, in the initial angular range of 1.5^o–3.0^o), combined with the value of the central magnetic field of the solenoid, provided a p/q determination with a resolution of ∼2%. Even though this resolution is not useful to improve the mass determination (as was done in the MARS data [46]), it was adequate to specify the charge state q of the ions.

As in the case of the MARS data, a series of runs at overlapping magnetic rigidity settings of the line in the range 1.1–1.6 T m for the ^{64}Ni (25MeV/nucleon) data and 1.0–1.5 T m for the ^{136}Xe (20 MeV/nucleon) data were performed. The data were normalized and appropriately combined, following the procedure described in [46]. Summation over all ionic charge states and, finally, normalization for beam current and target thickness, provided the fragment yield distributions with respect to Z, A and velocity. As in the case of the MARS data, the fragment yield distributions were summed over velocities and used to obtain the yield ratios for isoscaling.

III. ISOSCALING AND EXCITATION ENERGY DATA FROM THE VARIOUS REACTIONS

From the measured fragment yield distributions, we construct the ratio $R_{21}(N,Z) = Y_2(N,Z)/Y_1(N,Z)$ of yields of a given projectile fragment (N,Z) from reactions 2 and 1 using the convention that index 2 refers to the more neutron-rich system and index 1 to the less neutron-rich one. The results of the reactions with each of the various beams are given in the following subsections.

A. ^{86}Kr (25MeV/nucleon) data (MARS)

Fig. 2 shows the yield ratios R_{21}(N,Z) as a function of fragment neutron number N for selected isotopes for the Kr+Ni reactions (top panel) and the Kr+Sn reactions (bottom panel). The different isotopes are shown by alternating filled and open symbols for clarity. For each element, an exponential function of the form $Cexp(\alpha\ N)$ was fitted to the data and is shown in Fig. 2 for the selected elements. In the semi-log representation, the straight lines for each element are parallel up to Z∼34 for Kr+Ni and up to Z∼28 for Kr+Sn. For heavier fragments from the Kr+Sn system, the fits to the data show gradual decrease in the slopes with increasing Z, a behavior that has been shown to manifest incomplete N/Z equilibration for the most peripheral events for this reaction whose projectile-like fragments were observed inside the grazing angle [35, 36].

In Fig. 3a, we present the slope parameters α of the exponential fits (obtained as described for Fig. 2) as a function of Z. For the Kr+Ni reactions (open symbols), the slope parameter α is constant in the whole range Z=12–36 at an average value α=0.254. For the Kr+Sn reactions, the parameter α is roughly constant with an average value of 0.415 in the range Z=12–28 and then it decreases for Z>28. In the case of the Kr+Ni systems under the present experimental conditions (observation outside the grazing angle), isoscaling holds essentially in the whole range of observed fragments. To obtain information about the excitation energy of the primary fragments from the present reactions, we will employ the correlation of the measured velocity with the atomic number [35]. Fig. 3b presents the average velocities of the fragments as a function of Z. Open symbols correspond to the ^{86}Kr+^{64}Ni reaction and closed symbols to the ^{86}Kr+^{124}Sn reaction. In this figure, we observe

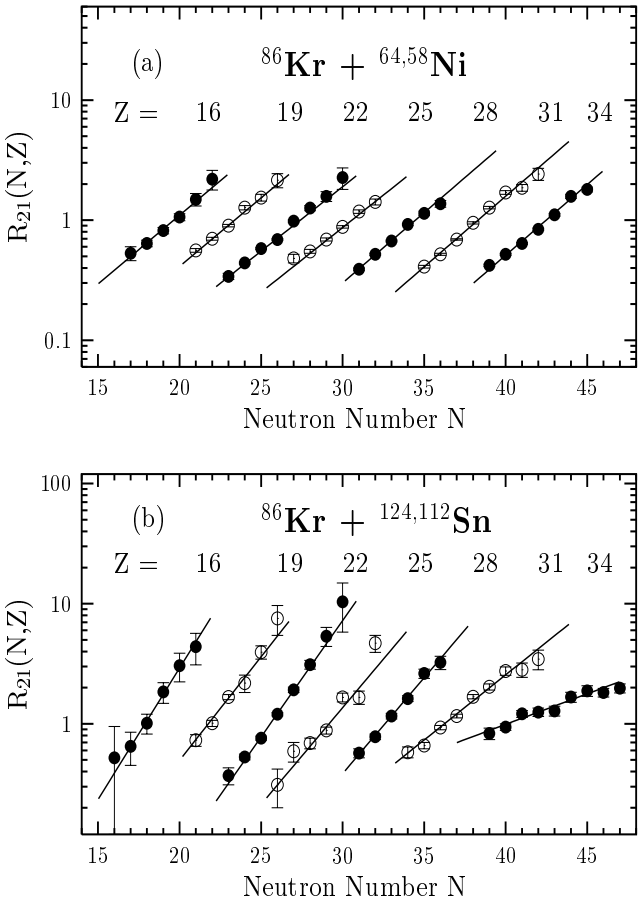

FIG. 2: (MARS data) Yield ratios $R_{21}(N,Z) = Y_2(N,Z)/Y_1(N,Z)$ of projectile residues from the reactions of ^{86}Kr (25 MeV/nucleon) with ^{64,58}Ni (a), and ^{124,112}Sn (b) with respect to N for the Z's indicated. The data are given by alternating filled and open circles, whereas the lines are exponential fits.

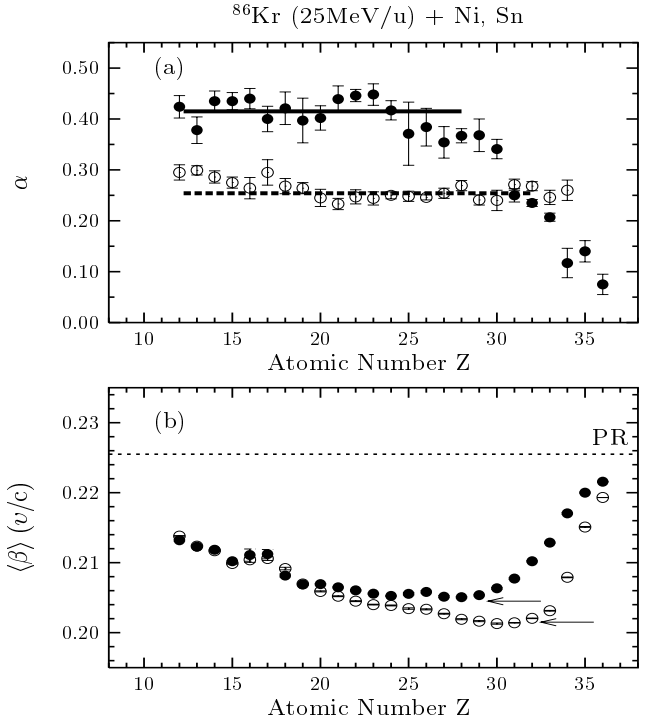

FIG. 3: (MARS data) (a) Isoscaling parameter α as a function of Z for projectile residues from the reactions of ^{86}Kr (25 MeV/nucleon) with ^{64,58}Ni (open circles) and ^{124,112}Sn (closed circles). The straight lines are constant value fits for each system. (b) Average velocity versus atomic number Z correlations for projectile residues from the reactions of ^{86}Kr (25 MeV/nucleon) with ^{64}Ni (open symbols) and ^{124}Sn (closed symbols). The dashed line (marked "PR") gives the velocity of the projectile, whereas the arrows indicate the minimum average residue velocities observed.

that for fragments close to the projectile, the velocities are slightly below that of the projectile, corresponding to very peripheral, low-excitation energy events. A monotonic decrease of velocity with decreasing Z is observed, indicative of lower impact parameters, and thus, higher excitation energies. For the ^{86}Kr+^{124}Sn reaction (closed symbols in Fig. 3b), the descending velocity–Z correlation continues down to Z∼28; for lower Z's, the velocity starts increasing with decreasing Z. A minimum velocity for Z∼28 can be understood by assuming that these residues originate from primary fragments with a maximum observed excitation energy. Fragments with Z near the projectile down to Z∼28 originate from evaporative type of deexcitation which does not modify, on average, the emission direction of the residues. Thus, the residue velocities provide information on the excitation energy. Residues with lower Z arise from primary fragments undergoing cluster emission and/or multifragmentation and the velocity of the inclusively measured fragments is not monotonically related to the excitation energy. For the ^{86}Kr+^{64}Ni reaction, a similar behavior is observed. However, the decreasing velocity–Z correlation is observed down to Z∼32. We remind that fragments from this reaction were measured mostly outside the grazing angle, so that they correspond to more damped collisions, in such a way that the final residues receive a larger recoil during the deexcitation and appear within this angular range. For Z∼30–32, we observe a minimum velocity and for lower Z's an increase of the velocity with decreasing Z analogous to the ^{86}Kr+^{124}Sn reaction. We mention that the average velocities from the reactions with the neutron-poor targets are, within the experimental uncertainties, almost the same as the corresponding from the reactions with the neutron-rich targets for both pairs of systems and are not shown in Fig. 3b. For both reactions, the ascending part of the velocity vs Z correlation for the lower part of the Z range is primarily due to the combined effect of angle and magnetic rigidity selection imposed by the spectrometer.

Employing the observed minimum velocities for the Kr+Ni and Kr+Sn reactions and, furthermore, assuming two-body kinematics, we can estimate the total excitation energy of the quasiprojectile – quasitarget sys-

tem employing standard mass tables [52]. In regards to the sharing of excitation energy, a reasonable assumption for peripheral/semiperipheral collisions is equal division [53, 54, 55] at relatively low kinetic energy losses, E_{loss}. This assumption was employed in our previous analysis of these isoscaling data [35]. In the present work, we use a more appropriate prescription in agreement with the experimentally observed transition of the excitation energy sharing from the equal division limit (at low E_{loss}) to the thermal limit that may be attained near the maximum of the kinetic energy loss, $E_{loss,max}$. Specifically, we estimate the fraction of the excitation energy of the quasi-projectile assuming a linear evolution, with respect to $E_{loss}/E_{loss,max}$, from the equal division limit to the thermal equilibrium limit. Following the above procedure, we can estimate an average excitation energy per nucleon for the hot quasiprojectile fragments of E^*/A = 2.4 MeV for the Kr+Ni system and E^*/A = 2.0 MeV for the Kr+Sn system (Table I). We note that, for these systems, the present estimates are close to the value E^*/A = 2.2 MeV obtained under the assumption of equal excitation energy division employed in our previous work [35].

B. ^{64}Ni (25MeV/nucleon) data (BigSol)

In Figs. 4 and 5, we show the data for the ^{64}Ni (25 MeV/nucleon) reactions obtained with the BigSol line. The presentation of the data follows a line similar to that of the MARS data (Figs. 2 and 3). In Figs. 4a,b, a general isoscaling behavior is seen in both the Ni+Ni (grazing angle θ_{gr}=3.8^o) and Ni+Sn (θ_{gr}=6.5^o) reactions essentially in the whole range of elements measured in the magnetic rigidity range 1.1–1.6 T m. A slight decrease of the isoscaling parameter α is discernible for near-projectile elements (Fig. 5a) possibly due to incomplete N/Z equilibration. Constant value fits to the α parameter vs Z in the range Z=12–24 yielded α=0.250 and 0.324 for Ni+Ni and Ni+Sn respectively (Table I).

For the ^{64}Ni + ^{232}Th, ^{208}Pb pair of reactions (θ_{gr}=9.5^o), we also observe isoscaling despite the small difference of ∼2.5% in the N/Z of the two systems (compared to, e.g., the ∼10% N/Z difference in the reaction pair of ^{64}Ni + ^{124}Sn,^{112}Sn). This limiting case shows the sensitivity of the isoscaling signal to the N/Z of the reacting systems. A constant value fit to the α parameter data of the Ni+Th,Pb pair in the region Z=14–18 (Fig. 5a) gives, as expected, a small value α=0.060 (Table I).

The average velocities of the three ^{64}Ni reactions are shown in Fig. 5b (only the neutron-rich systems are presented). As we see in the figure, near-projectile residues with velocities close to that of the projectile were not collected in these measurements, mainly due to magnetic rigidity selection (and, in addition, due to angle selection $\Delta\theta$=1.5–3.0^o, particularly for the Ni+Th,Pb systems with θ_{gr}=9.5^o). In a manner similar to the MARS data, we employed the observed minimum velocities to extract average excitation energies for the fragmenting Ni-like quasiprojectiles resulting in a common value of E^*/A = 2.9 MeV for the three pairs of the ^{64}Ni reactions (Table I).

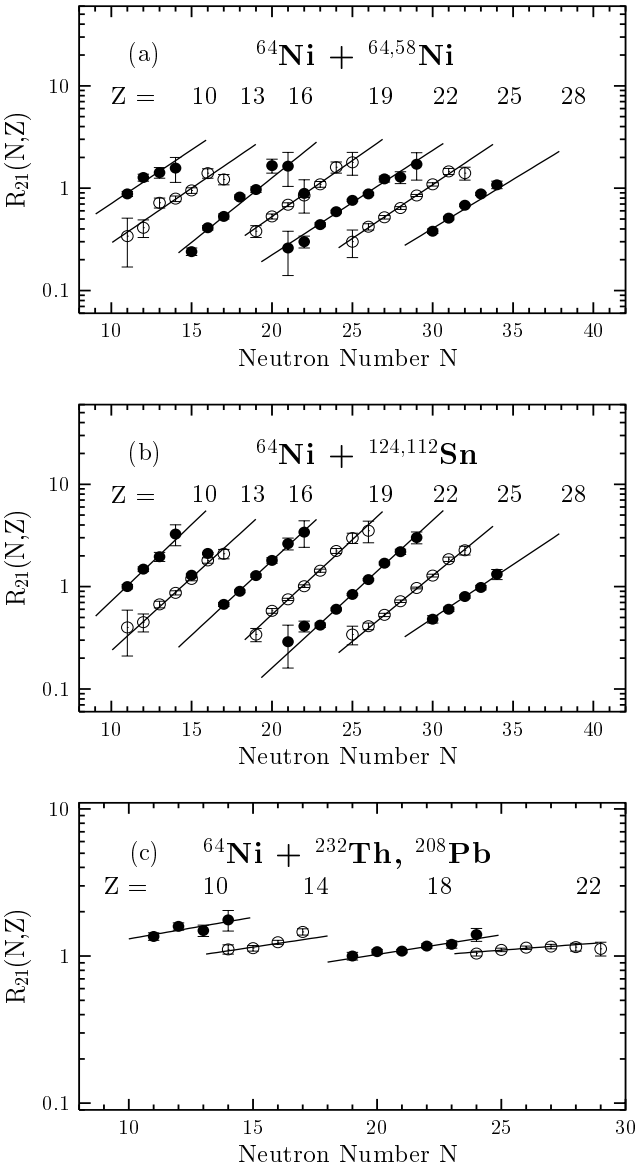

FIG. 4: (BigSol data) Yield ratios $R_{21}(N,Z) = Y_2(N,Z)/Y_1(N,Z)$ of projectile residues from the reactions of ^{64}Ni (25 MeV/nucleon) with ^{64,58}Ni (a), ^{124,112}Sn (b), and ^{232}Th,^{208}Pb (c) with respect to N for the Z's indicated. The data are given by alternating filled and open circles, whereas the lines are exponential fits.

C. ^{136}Xe (20 MeV/nucleon) data (BigSol)

Finally, in Figs. 6 and 7, we present the data for the reactions of the ^{136}Xe (20 MeV/nucleon) beam on the three pairs of targets ^{64,58}Ni, ^{124,112}Sn and ^{232}Th, ^{197}Au obtained with the BigSol line. Again, the presentation

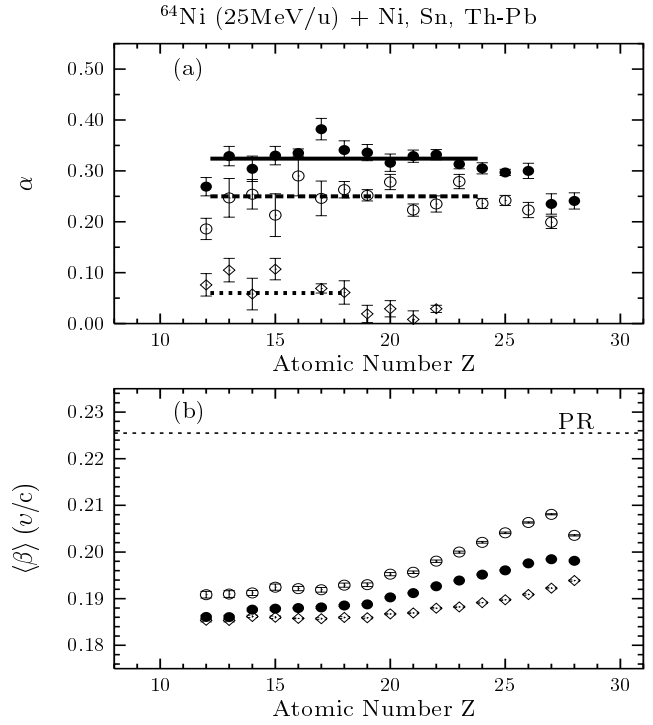

FIG. 5: (BigSol data) (a) Isoscaling parameter α as a function of Z for projectile residues from the reactions of ^{64}Ni (25 MeV/nucleon) with ^{64,58}Ni (open circles), ^{124,112}Sn (closed circles), and ^{232}Th,^{208}Pb (open diamonds). The straight lines are constant value fits for each system. (b) Average velocity versus atomic number Z correlations for projectile residues from the reactions of ^{64}Ni(25 MeV/nucleon) with ^{64}Ni (open symbols), ^{124}Sn (closed symbols), and ^{232}Th (open diamonds). The dashed line (marked "PR") gives the velocity of the projectile.

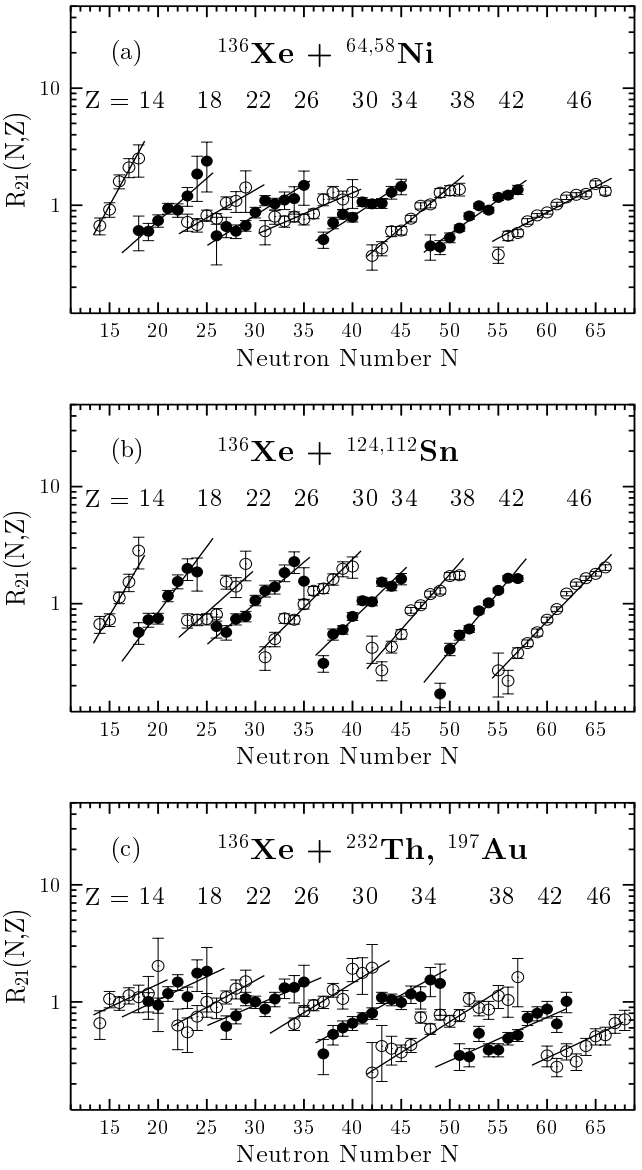

FIG. 6: (BigSol data) Yield ratios $R_{21}(N,Z) = Y_2(N,Z)/Y_1(N,Z)$ of projectile residues from the reactions of ^{136}Xe (20 MeV/nucleon) with ^{64,58}Ni (a), ^{124,112}Sn (b), and ^{232}Th,^{197}Au (c) with respect to N for the Z's indicated. The data are given by alternating filled and open circles, whereas the lines are exponential fits.

of the data is similar to that of the preceding sections. Fig. 6 shows the isoscaling behavior of the yields and the fits to selected elements. Fig. 7a shows the variation of the isoscaling parameter α as a function of Z. The α values for Xe+Ni and Xe+Sn are displaced vertically for viewing. Despite the relatively large fluctuation in the data points, the data were fitted with straight lines in the region Z=14–46 yielding the values: 0.129, 0.193, and 0.096 for the three reaction pairs, respectively (Table I).

Fig. 7b shows the average velocities of the three ^{136}Xe reactions (again, only the neutron-rich systems are presented). The grazing angles for these systems are 3.9^o, 6.3^o and 10.0^o respectively. The angle and magnetic rigidity selection were such that near-projectile residues with velocities close to that of the projectile were not collected, as in the case of the ^{64}Ni reactions. However, the kinematical conditions were such that lighter fragments (below Z=35) show an ascending velocity behavior with decreasing Z analogous to the one observed in the Kr+Ni,Sn reactions (Fig. 3b). Using the observed minimum velocities, average excitation energies for the fragmenting Xe-like quasiprojectiles were extracted resulting again in a common value of E*/A = 2.5 MeV for the three pairs of the ^{136}Xe reactions.

IV. INTERPRETATION OF RESULTS AND DISCUSSION

Before proceeding to the analysis and interpretation of the present results on heavy fragment isoscaling, we present a summary of the reactions and the relevant parameters in Table I. The difference in the isotopic composition, expressed as the proton fraction squared, $(Z/A)^2$,

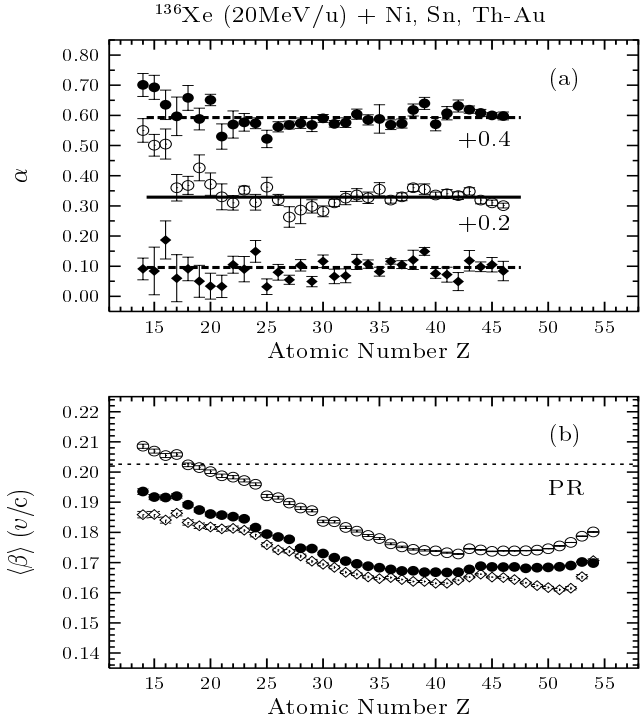

FIG. 7: (BigSol data) (a) Isoscaling parameter α as a function of Z for projectile residues from the reactions of ^{136}Xe (20 MeV/nucleon) with ^{64,58}Ni (open circles), ^{124,112}Sn (closed circles), and ^{232}Th,^{208}Pb (closed diamonds). The values of the first two systems are displaced vertically by +0.4 and +0.2 units, respectively, for viewing. The straight lines are constant value fits for each system. (b) Average velocity versus atomic number Z correlations for projectile residues from the reactions of ^{136}Xe (20 MeV/nucleon) with ^{64}Ni (open symbols), ^{124}Sn (closed symbols), and ^{232}Th (open diamonds). The dashed line (marked "PR") gives the velocity of the projectile.

for each pair of systems is given along with the excitation energies (obtained from residue velocities), as well as the temperatures (calculated with the Fermi gas model and the expanding mononucleus model [56], as discussed below). The isoscaling parameters α and, finally, the extracted values of the symmetry energy coefficient are summarized.

A. Determination of temperature

In order to estimate the temperature of the fragmenting quasiprojectiles using the measured average excitation energies, we first employ the simple Fermi gas relationship of the form $E^* = \frac{A}{K}T^2$, with T the tempretature and K the inverse level density parameter. It is well known that for the non-interacting Fermi gas model the value of the inverse level density parameter is K $\simeq$16 (e.g. [57]), whereas the experimental data are consistent with lower values of K dependent on both the excitation energy and the mass range [58]. For the present systems in the 2–3 MeV/nucleon excitation range, values in the vicinity of K=12–13 are consistent with the experimental systematics [58]. Given the expected mass and excitation energy dependence of K, we decided to use values of K following the model of Shlomo and Natowitz [59, 60]. This model determines the nuclear level density within the framework of the Fermi gas incorporating the effects of the finite size of the nucleus, the contributions of the continuum states and the temperature and density dependence of the nucleon effective mass. For the hot quasiprojectiles (Kr-like, Ni-like and Xe-like) of the present work, the values of K reported in Table I were

TABLE I: Summary of reaction pairs studied in this work (see text), along with parameters relevant to the isoscaling analysis: $\Delta(Z/A)^2$ difference in $(Z/A)^2$ of the two reactions of each pair. E^*/A (MeV): excitation energy per nucleon of the corresponding primary quasiprojectiles. K (MeV): inverse level density parameter. T_F, T_m(MeV): temperature estimates obtained from the Fermi gas model and the expanding mononucleus model [56]. α: isoscaling parameter. $c \equiv \alpha/\Delta(Z/A)^2$: reduced isoscaling parameter. $C_{sym,F}$, $C_{sym,m}$ (MeV): symmetry energy coefficient of the nuclear binding energy obtained using the two temperature determinations T_F and T_m respectively, as mentioned above. Errors (one standard deviation) of the measured quantities are given in parentheses.

Reaction	$\Delta(Z/A)^2$	E^*/A	K	T_F	T_m	α	c	$C_{sym,F}$	$C_{sym,m}$
Kr+Sn	0.0209	2.0	11.5	4.8	3.9	0.415	19.9	23.9	19.4
		(0.1)				(0.010)	(0.5)	(0.6)	(0.5)
Kr+Ni	0.0154	2.4	11.8	5.3	4.2	0.254	16.5	21.9	17.2
		(0.1)				(0.005)	(0.3)	(0.5)	(0.4)
Ni+Ni	0.0193	2.9	11.7	5.8	4.3	0.250	13.0	18.9	14.0
		(0.1)				(0.007)	(0.4)	(0.6)	(0.4)
Ni+Sn	0.0240	2.9	11.7	5.8	4.3	0.324	13.5	19.6	14.5
		(0.1)				(0.005)	(0.3)	(0.5)	(0.4)
Ni+Th–Pb	0.0046	2.9	11.7	5.8	4.3	0.060	13.0	18.9	14.0
		(0.1)				(0.010)	(2.2)	(3.2)	(2.2)
Xe+Ni	0.0106	2.5	13.5	5.8	4.5	0.129	12.2	17.7	13.7
		(0.1)				(0.006)	(0.6)	(0.9)	(0.7)
Xe+Sn	0.0159	2.5	13.5	5.8	4.5	0.193	12.1	17.6	13.6
		(0.1)				(0.005)	(0.3)	(0.5)	(0.4)
Xe+Th–Au	0.0064	2.5	13.5	5.8	4.5	0.096	15.0	21.8	16.9
		(0.1)				(0.005)	(0.8)	(1.2)	(0.9)

obtained by interpolating the results presented in Fig. 1 of [59]. The corresponding values of the temperature are also listed under the column T_F and discussed later in relation to Figs. 9b and 9c. These temperature values are in reasonable overall agreement with measured temperatures of similar systems in this excitation energy range, as systematically analyzed and presented in [58].

In addition to the above procedure to obtain the temperature of fragmenting quasiprojectiles, we wish to investigate the possible effect of expansion of the hot nucleus in the temperature determination and, subsequently, in the extraction of the symmetry energy coefficient. For this purpose we employed the recently developed expanding mononucleus model of Sobotka and T$\bar{o}$ke [56]. Compared with the above non-expanding Fermi gas framework [57], this model incorporates the expansion as a degree of freedom [61]. The effect of the variation the nucleon effective mass in the level density is included in a manner analogous to [57]. For a given excitation energy E^*/A, the collective expansion energy is taken into account. The compressibility is chosen to correspond to a soft equation of state. The density of the mononucleus is determined so that it maximizes the entropy. The temperature, in turn, is obtained from the maximum entropy state. Using this model, we calculated the values of the temperature for the quasiprojectiles of the reactions studied in this work which are summarized in Table I under the column T_m and later presented in Fig. 9. As we observe in Table I (and in Fig. 9b), the temperatures obtained with this model are systematically lower that those obtained from the (non-expanding) Fermi gas model. Despite differences in the details of the two models, this difference may be understood qualitatively as the effect of expansion: in the expanding mononucleous model, part of the available excitation energy is allocated as potential energy of expansion, leaving the rest of the amount as thermal energy and, thus, leading to lower temperature. For completeness in the following discussion, both approaches for the determination of the temperature will be employed, and the respective results of the symmetry energy coefficient will be presented and discussed.

B. Determination of the symmetry energy coefficient

Having studied the isoscaling behavior and determined the corresponding excitation energies and temperatures, we currently turn our discussion to the possibility of obtaining information on the symmetry energy and its dependence on excitation energy. The key quantity for this effort is the isoscaling parameter α. It has been shown [28, 30, 32] that the isoscaling parameter α is directly related to the coefficient C_{sym} of the symmetry energy term $E_{sym} = C_{sym}(N-Z)^2/A$ of the nuclear binding energy. The following relation has been obtained in the framework of the grand canonical limit of the statistical multifragmentation model (SMM) [32], in the expanding–emitting source (EES) model [30, 31] and in the framework of dynamical calculations with the AMD model [28, 42]:

$$\alpha = 4\,\frac{C_{sym}}{T}((\frac{Z}{A})_1^2 - (\frac{Z}{A})_2^2) \qquad (2)$$

where the atomic number Z and the mass number A refer to the fragmenting quasiprojectiles from reactions 1 and 2.

In principle, Eq. 2 can serve as the basis for determining the symmetry energy coefficient C_{sym} for expanded multifragmenting quasiprojectiles. For this purpose, the isoscaling parameter α, the isotopic composition and the temperature of fragmenting quasiprojectiles should be determined. From the present study of heavy fragment isoscaling, the values of the isoscaling parameter α have been extracted for each reaction pair, as already discussed. The difference in isospin asymmetry between quasiprojectiles of each reaction pair is taken to be equal to that of the combined (fully mixed) system. We assumed that N/Z equilibration has been reached in the present reactions at the energy range 20–25 MeV/nucleon, as suggested by recent experimental studies [36] and calculations [62]. In addition, in peripheral collisions at these bombarding energies, the effect of pre-equilibrium emission does not appreciably change the difference in isospin asymmetry, as has been concluded by calculations using the model framework of [63]. The same conclusion has also been reached in the recent isoscaling studies of spectator fragmentation at higher energies [40]. Finally, it should be noted that the effect of secondary decay on the values of the isoscaling parameter α in the excitation energy range $E^*/A < 3$ MeV is expected to be small [64]. Thus, by using the experimental isoscaling parameter α, the temperature and the difference in isospin asymmetry obtained as described above, we can obtain the values of the symmetry energy coefficient C_{sym} for each case corresponding to the various values of the excitation energy, as summarized in Table I. In the following, we will discuss in further detail the steps involved to extract C_{sym} with the help of Figs. 8 and 9.

Fig. 8 presents the experimental values of the isoscaling parameter α for the various systems studied in this work as a function of the difference in isospin composition of each pair of reactions expressed as $(\frac{Z}{A})_1^2 - (\frac{Z}{A})_2^2$. The various symbols correspond to the reactions studied as explained in the caption of the figure. It is interesting to point out the linear relationship of the three points of the ^{64}Ni data, all of which have approximately the same excitation energy of 2.9 MeV/nucleon. A similar observation can be made for the ^{136}Xe data points, which correspond to a common excitation energy of 2.5 MeV/nucleon.

Using the values of α and $(\frac{Z}{A})_1^2 - (\frac{Z}{A})_2^2$, we obtain the parameter:

$$c \equiv \frac{\alpha}{(\frac{Z}{A})_1^2 - (\frac{Z}{A})_2^2} \qquad (3)$$

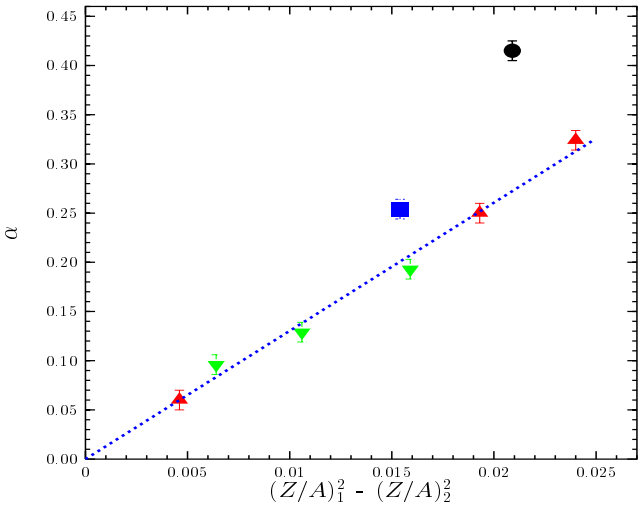

FIG. 8: (Color online) Isoscaling parameter α as a function of $(Z/A)_1^2 - (Z/A)_2^2$ for each reaction pair studied (see text). Circle: ^{86}Kr + ^{124,112}Sn. Square: ^{86}Kr + ^{64,58}Ni. Upright triangles: ^{64}Ni + ^{124,112}Sn, ^{64,58}Ni, ^{232}Th–^{208}Pb, respectively in decreasing values of α. Inverted triangles: ^{136}Xe + ^{124,112}Sn, ^{64,58}Ni, ^{232}Th–^{197}Au, respectively in decreasing values of α. The straight dotted line indicates the linear relationship of the ^{64}Ni points (see text).

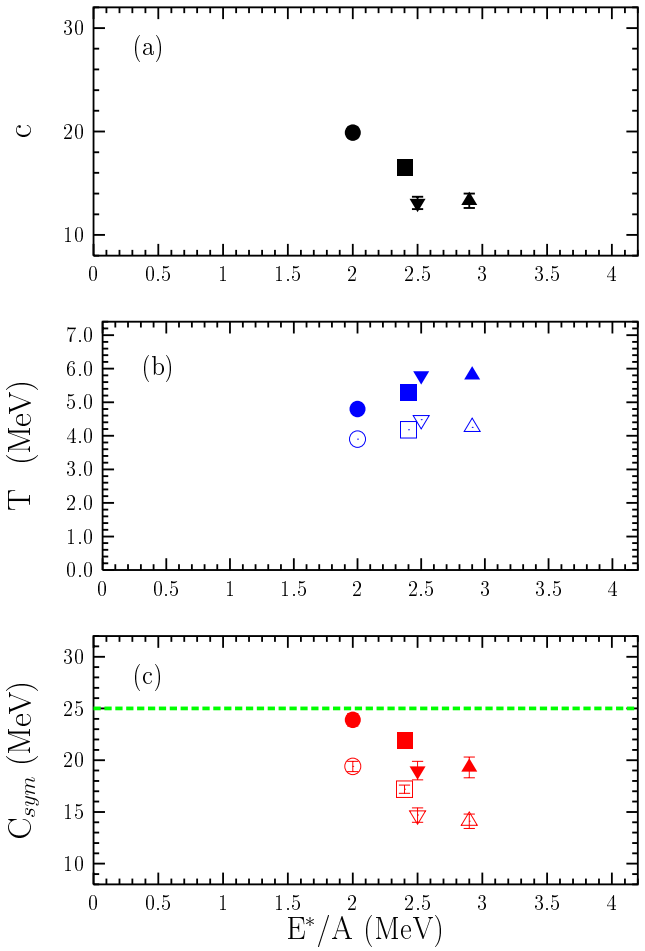

FIG. 9: (Color online) (a) Reduced isoscaling parameter $c \equiv \alpha/((Z/A)_1^2 - (Z/A)_2^2)$ as a function E*/A. Circle: ^{86}Kr + ^{124,112}Sn. Square: ^{86}Kr + ^{64,58}Ni. Upright triangle: ^{64}Ni reactions. Inverted triangle: ^{136}Xe reactions. (b) Temperature as a function of E*/A. Open symbols: Fermi gas. Closed symbols: expanding mononucleus model [56]. Symbol types as in (a). (c) Symmetry energy coefficient C_{sym} as a function of E*/A. Open and closed symbols correspond to the two temperature estimates as in (b). Symbol types as in (a). The horizontal dashed line indicates the typical value of C_{sym} for cold nuclei.

which we call "reduced" isoscaling parameter. The values of c with respect to the corresponding excitation energies are shown in Fig. 9a. Because of the common excitation energy for the three ^{64}Ni reaction pairs (and similarly for the three ^{136}Xe pairs), we plotted the corresponding average values of c in Fig. 9a.

Fig. 9b shows the temperatures calculated both with the Fermi gas model (closed symbols) and the expanding mononucleus model (open symbols). As already mentioned, the temperature values calculated with the mononucleus expansion model are systematically lower (and appear to lead to a plateau with respect to excitation energy, as also discussed in [56]).

From Eq. 2, with the definition of Eq. 3, for the symmetry energy coefficient we simply have:

$$C_{sym} = \frac{cT}{4} \qquad (4)$$

The values of C_{sym} obtained using this equation are shown in Fig. 9c with closed symbols (using the Fermi gas temperature) and open symbols (using the expanding mononucleus temperature). As previously discussed, the simple (non-expanding) Fermi gas temperatures are in overall agreement with the existing experimental systematics, thus the extracted values of C_{sym} should be considered the most appropriate ones for the present analysis. Obviously, the values of the symmetry energy coefficient obtained using the expanding mononucleus temperature are, as expected, systematically lower. However, within both sets of C_{sym} values, a decreasing trend with increasing excitation energy is clearly observed. In the following, only the values of C_{sym} corresponding to the Fermi gas temperatures will be discussed further.

From Fig. 9c (closed symbols), we observe that, at excitation energy E*/A $\sim$ 2.0 MeV, the value of the symmetry energy coefficient is near (slightly lower than) the conventional value $C_{sym,0} \simeq 25$ MeV for cold (unexpanded) nuclei. With increasing excitation energy, however, C_{sym} appears to decrease monotonically. The observed considerable decrease of the symmetry energy coefficient with excitation energy towards the multifragmentation regime is in overall qualitative agreement with the conclusions of Shetty et al. [64], Le Fèvre et al. [40] and Henzlova et al. [41]. We wish to point out, however, that the present study of heavy residue isoscaling reveals the gradual de-

crease of the symmetry energy C_{sym} with increasing excitation energy in the range E^*/A=2.0–2.9 MeV.

The observed decrease in the fragment symmetry energy with increasing excitation has important consequences for the formation of hot primary fragments and, as recently shown in [65], their subsequent decay. Similar hot nuclei are also produced in the interior of a collapsing star and subsequent supernova explosion [66**?**]. In these works it is predicted that a small decrease in the symmetry energy coefficient can significantly alter the elemental abundance and the synthesis of heavy elements in type II supernova. In light of this intimate connection, the present measurements and results can provide an important testing ground to study the role of the symmetry energy in the formation and decay of hot fragments and, subsequently, to implement this knowledge in the simulation of the distribution of hot exotic nuclei in supernova and other hot and dense stellar environments. Along these lines, a thorough comparison of the isoscaling properties and the N/Z characteristics of the residues of the present work with the statistical multifragmentation model (SMM) [67] is currently underway.

C. Final remarks and future directions

As concluding remarks from this study, we point out that the present mass spectrometric data provided information on the isoscaling properties of heavy projectile fragments and, in parallel, information on the average excitation energy of the primary fragments (via residue velocity measurements). These two main experimental observables were used in the analysis presented in this work to extract the symmetry energy coefficient at the corresponding excitation energy. An important advantage associated with the detailed study of heavy residues is that, in the respective excitation energy range $E^*/A < 3$ MeV, the effect of de-excitation on the isoscaling parameter α is expected to be small, as discussed earlier, thus slightly affecting the procedure to obtain the symmetry energy coefficient. As a future experimental step, we wish to propose the combination of a mass separator/spectrometer with a multidetector system capable of providing full acceptance and characterization for all fragments of the decaying projectile. Such an apparatus could enable the determination of the excitation energy on an event-by-event basis, along with temperature measurements via standard double-isotope techniques [58]. This way, a detailed mapping of the excitation energy could be performed for various reaction pairs covering the whole range from low excitation energies (where only heavy residues are present that can be separated and identified with the spectrometer) to the multifragmentation region. At each excitation energy bin, the isoscaling parameter α and the temperature can be obtained. In addition, these measurements can be supplemented by efforts to determine the density (e.g., following approaches as discussed in [68] and [69]). Consequently, a correlation of the symmetry energy coefficient with excitation energy and, possibly, density may be obtained. Finally, such advanced experimental studies can be extended to the limits of isospin by taking advantage of present and future developments of rare isotope beams.

V. SUMMARY AND CONCLUSIONS

The isoscaling properties of isotopically resolved projectile residues from peripheral collisions of ^{86}Kr (25MeV/nucleon), ^{64}Ni (25MeV/nucleon) and ^{136}Xe (20MeV/nucleon) beams on various target pairs are employed to probe the symmetry energy term of the nuclear binding energy of hot fragments. The reactions of ^{86}Kr with ^{64,58}Ni and ^{124,112}Sn were studied with the MARS recoil separator. The reactions of ^{64}Ni and ^{136}Xe with ^{64,58}Ni and ^{124,112}Sn, as well as heavier targets (^{197}Au, ^{208}Pb, ^{232}Th) were studied with the Superconducting Solenoid Line (BigSol) at the Cyclotron Institute of Texas A&M University. The present study focused on heavy projectile fragments produced in peripheral and semiperipheral collisions near the onset of multifragment emission (E^*/A = 2–3 MeV). For these fragments, the measured average velocities were used to extract excitation energies. The excitation energies, in turn, are employed to estimate the temperatures of the fragmenting quasiprojectiles within the framework of the Fermi gas model. The isoscaling analysis of the fragment yields provided the isoscaling parameters α which, combined with temperatures and isospin asymmetries, provided the values of the symmetry energy. The extracted value of the symmetry energy coefficient C_{sym} at $E^*/A \simeq 2$ MeV is near (just below) the typical value $\sim$25 MeV and is found to decrease monotonically with further increase of the excitation energy. The observed decrease of C_{sym} with excitation energy is of significant importance to the understanding of the formation and decay of hot nuclei not only in nuclear multifragmentation, but also in supernova and other hot stellar environments.

VI. ACKOWLEDGEMENTS

We wish to thank A. S. Botvina for fruitful and enlightening discussions at various stages of this work. We are thankful to L. G. Sobotka for providing us with his code on expanding mononucleus calculations. We are grateful to F. D. Becchetti and T. W. O'Donnel for valuable advise and discussions during the setup and commissioning of the Superconducting Solenoid Line at the Cyclotron Institute of Texas A&M University. Finally, we wish to thank the Cyclotron Institute staff for the excellent beam quality. This work was supported in part by the Robert A. Welch Foundation through grant No. A-1266, and the Department of Energy through grant No. DE-FG03-93ER40773. M.V. was also supported through grant VEGA-2/5098/25 (Slovak Scientific Grant

Agency).

[1] A. W. Steiner, M. Prakash, J. M. Lattimer, and P. Ellis, Phys. Rep. **411**, 325 (2005).
[2] C. Lee, Phys. Rep. **275**, 255 (1996).
[3] H. A. Bethe, Rev. Mod. Phys. **62**, 801 (1990).
[4] C. J. Pethick and D. G. Ravenhall, Annu. Rev. Nucl. Part. Sci. **45**, 429 (1995).
[5] J. M. Lattimer and M. Prakash, Phys. Rep. **333**, 121 (2000).
[6] W. R. Hix et al., Phys. Rev. Lett. **91**, 201102 (2003).
[7] J. R. Stone et al., Phys. Rev. C **68**, 034324 (2003).
[8] A. S. Botvina and I. N. Mishustin, Phys. Lett. B **584**, 233 (2004).
[9] K. Oyamatsu et al., Nucl. Phys. A **634**, 3 (1998).
[10] B. A. Brown, Phys. Rev. Lett. **85**, 5296 (2000).
[11] C. J. Horowitz and J. Piekarewicz, Phys. Rev. Lett. **86**, 5647 (2001).
[12] R. J. Furnstahl, Nucl. Phys. A **706**, 85 (2002).
[13] D. T. Khoa, W. von Oertzen, and A. A. Oglobin, Nucl. Phys. A **602**, 98 (1996).
[14] W. Zuo, I. Bombaci, and U. Lombardo, Phys. Rev. C **60**, 024605 (1999).
[15] M. Brack, C. Guet, and H. B. Hakansson, Phys. Rep. **123**, 276 (1985).
[16] J. M. Pearson and R. C. Nayak, Nucl. Phys. A **668**, 163 (2000).
[17] A. E. L. Dieperink et al., Phys. Rev. C **68**, 064307 (2003).
[18] W. D. Myers and W. J. Swiatecki, Nucl. Phys. **81**, 1 (1966).
[19] K. Pomorski and J. Dudek, Phys. Rev. C **67**, 044316 (2003).
[20] J. R. Stone et al., J. Phys. G, Nucl. Part. Phys. **31**, 211 (2005).
[21] D. Lunney, J. M. Pearson, and C. Thibault, Rev. Mod. Phys. **75**, 1021 (2003).
[22] D. V. Shetty, S. J. Yennello, and G. A. Souliotis, nucl-ex/0505011 (2005).
[23] D. V. Shetty et al., Phys. Rev. C **70**, 011601 (2004).
[24] L. W. Chen, C. M. Ko, and B. A. Lee, Phys. Rev. Lett. **94**, 032701 (2005).
[25] D. T. Khoa and H. S. Than, Phys. Rev. C. **71**, 044601 (2005).
[26] B.-A. Li, C. M. Ko, and W. Bauer, Int. J. Mod. Phys. E **7**, 147 (1998).
[27] B.-A. Li and W. U. Schroeder, eds., *Isospin Physics in Heavy Ion Collisions at Intermediate Energies* (Nova Science, New York, 2001).
[28] A. Ono et al., Phys. Rev. C **68**, 051601 (2003).
[29] Y. Zhang and Z. Li, Phys. Rev. C **71**, 024604 (2005).
[30] M. B. Tsang et al., Phys. Rev. Lett. **86**, 5023 (2001).
[31] M. B. Tsang et al., Phys. Rev. C **64**, 054615 (2001).
[32] A. S. Botvina, O. V. Lozhkin, and W. Trautmann, Phys. Rev. C **65**, 044610 (2002).
[33] M. Veselsky, G. A. Souliotis, and M. Jandel, Phys. Rev. C **69**, 044607 (2004).
[34] W. A. Friedman, Phys. Rev. C **69**, 031601 (2004).
[35] G. A. Souliotis et al., Phys. Rev. C **68**, 024605 (2003).
[36] G. A. Souliotis et al., Phys. Lett. B **588**, 35 (2004).
[37] D. V. Shetty et al., Phys. Rev. C **68**, 021602 (2003).
[38] M. Veselsky, G. A. Souliotis, and S. J. Yennello, Phys. Rev. C **69**, 031602 (2004).
[39] E. Geraci et al., Nucl. Phys. A **732**, 173 (2004).
[40] A. LeFèvre et al., Phys. Rev. Lett. **94**, 162701 (2005).
[41] D. Henzlova et al., nucl-ex/0507003 (2005).
[42] A. Ono et al., Phys. Rev. C **70**, 041604 (2004).
[43] R. E. Tribble, R. H. Burch, and C. A. Gagliardi, Nucl. Instrum. Methods Phys. Res. A **285**, 441 (1989).
[44] W. W. Wilcke et al., At. Data Nucl. Data Tables **25**, 389 (1980).
[45] G. A. Souliotis et al., Phys. Rev. Lett. **91**, 022701 (2003).
[46] G. A. Souliotis et al., Phys. Lett. B **543**, 163 (2002).
[47] G. A. Souliotis et al., Nucl. Instrum. Methods Phys. Res. B **204**, 166 (2003).
[48] T. W. O'Donnell, Ph. D. Thesis, university of Michgan; http://www-personal.umich.edu/∼twod/thesis/ (2000).
[49] T. W. O'Donnell et al., Nucl. Instrum. Methods Phys. Res. A **422**, 513 (1999).
[50] G. A. Souliotis et al., Progress in Research, Cyclotron Institute, Texas A&M University (2003-2004), p. II-26; ibid (2002-2003) p. V-5; ibib (2001-2002) p. V-19; accessible at: http://cyclotron.tamu.edu (2005).
[51] H. Geissel and G. Munzenberg, Annu. Rev. Nucl. Part. Sci. **45**, 163 (1995).
[52] P. Moller, J. R. Nix, and K. L. Kratz, At. Data Nucl. Data Tables **66**, 131 (1997).
[53] H. Madani et al., Phys. Rev. C **54**, 1291 (1996).
[54] J. Tõke and W. U. Schroeder, Annu. Rev. Nucl. Part. Sci. **42**, 401 (1992).
[55] M. Veselsky et al., Phys. Rev. C **62**, 064613 (2000).
[56] L. G. Sobotka et al., Phys. Rev. Lett. **93**, 132702 (2004).
[57] S. Shlomo and V. M. Kolomietz, Rep. Prog. Phys. **68**, 1 (2005).
[58] J. B. Natowitz et al., Phys. Rev. C **65**, 034618 (2002).
[59] S. Shlomo and J. B. Natowitz, Phys. Rev. C **44**, 2878 (1991).
[60] S. Shlomo and J. B. Natowitz, Phys. Lett. B **252**, 187 (1990).
[61] J. Tõke, J. Lu, and W. U. Schroeder, Phys. Rev. C **67**, 034609 (2003).
[62] B.-A. Li and S. J. Yennello, Phys. Rev. C **52**, 1746 (1995).
[63] M. Veselsky, Nucl. Phys. A **705**, 193 (2002).
[64] D. V. Shetty et al., Phys. Rev. C **71**, 024602 (2005).
[65] N. Buyukcizmeci, R. Ogul, and A. S. Botvina, Eur. Phys. Jou. A **25**, 57 (2005).
[66] A. S. Botvina and I. N. Mishustin, Phys. Rev. C **72**, 048801 (2005).
[67] J. P. Bondorf et al., Phys. Rep. **257**, 133 (1995).
[68] J. B. Natowitz et al., Phys. Rev. C **66**, 031601 (2002).
[69] V. Viola et al., Phys. Rev. Lett. **93**, 132701 (2004).